Charge symmetry breaking in the $np \to d\pi^0$ reaction

Daniel R. Bolton and Gerald A. Miller
Department of Physics, University of Washington, Seattle, Washington 98195-1560, USA
(Received 11 October 2009; published 8 January 2010)

The asymmetry in the angular distribution of $np \to d\pi^0$ attributable to charge symmetry breaking is calculated using heavy baryon chiral perturbation theory. Recent developments in power counting have proven successful in describing total cross sections, and we apply them to the asymmetry calculation. Reducibility in one of the leading-order diagrams is examined. We compare the updated theory with experimental results for a range of physically reasonable parameters and find overprediction for the entire range.

DOI: 10.1103/PhysRevC.81.014001 PACS number(s): 11.30.Er, 24.80.+y, 25.10.+s

I. INTRODUCTION

The nuclear reaction $NN \to NN\pi$ has been studied for a long time in many ways. Theoretical understanding of the reaction is currently pursued using heavy baryon chiral perturbation theory (HBχPT) [1–4]. This effective theory of the strong nuclear force treats hadrons and mesons as the fundamental degrees of freedom. The Lagrangian contains an infinite number of terms that decrease in importance according to an expansion in a (somewhat) small parameter. Such an understanding is important because it is model independent, provided convergence is achieved. Furthermore, once theorists arrive at an ordering scheme for the expansion, error estimates will become more reliable and calculations of different and more exotic reactions will become possible.

One particularly interesting observable that HBχPT can help determine is the magnitude of charge symmetry breaking (CSB) [5–7]. Charge symmetry refers to the approximate invariance of hadronic systems under an isospin rotation of π about the y axis. This symmetry is broken by the mass difference between up and down quarks and by electromagnetic effects [8]. We will discuss the corresponding symmetry breaking terms in the HBχPT Lagrangian. These terms are especially important for the interactions of neutral pions [9].

Relations involving the light quark masses can be obtained from the SU(3) chiral symmetry on which HBχPT is based, but experiments that directly measure $m_d - m_u$ are difficult because of the lack of a neutral pion beam. One experiment that overcomes this difficulty and also minimizes electromagnetic effects is $np \to d\pi^0$. The angular distribution of this reaction is symmetric about 90° in the center of mass when charge symmetry is respected. Reference [10] recently observed that this distribution is asymmetric.

This report advances previous work in several ways. The authors of Ref. [11] showed that a vertex that was thought to be higher order in fact contributes at leading order. This led to a much improved understanding of the total cross section of $pp \to d\pi^+$. We extend this calculation off threshold for neutral pion production and make a comparison with the corresponding data. We also investigate a subtlety regarding reducibility in one of the leading-order diagrams and comment on the resulting corrections. Finally, we calculate the asymmetry of $np \to d\pi^0$, bringing up to date the calculations of Refs. [12] and [13] by including the new effects discussed in this paragraph.

In Sec. II we discuss the kinematics and selection rules of the $np \to d\pi^0$ process. Then, in Sec. III we develop the formalism necessary for calculation of the cross section. Here we detail the procedure for handling strongly interacting initial and final states. In Sec. IV we present the leading-order diagrams with vertices from the isospin conserving part of the Lagrangian (Appendix A). In this section we also provide a review of the power counting developed by Ref. [11] and discuss its impact on neutral pion production. Next, in Sec. V, we present diagrams with vertices from the CSB part of the Lagrangian which contribute to the reaction. Our results are given in Sec. VI and discussed in Sec. VII. Also in Sec. VII, we compare our work with another recent calculation of the asymmetry in Ref. [14].

II. KINEMATICS AND SELECTION RULES

At threshold, the reaction $NN \to NN\pi$ produces a pion from the kinetic energy of the incoming NN pair. Let $\vec{p} = \frac{1}{2}(\vec{p}_1 - \vec{p}_2)$ be the relative momentum of the pair. In the center of mass frame for this reaction, the total momentum $\vec{P} = \vec{p}_1 + \vec{p}_2 = 0$ and thus $\vec{p}_1 = \vec{p}$ and $\vec{p}_2 = -\vec{p}$. In the nonrelativistic limit, the total initial energy is $E_i = 2M_N + p^2/M_N$, where M_N is the nucleon mass (the average mass is used for np reactions). The energy of the final state at threshold is $E_f = 2M_N - E_b + m_\pi$, where $E_b = 2.224$ MeV is the deuteron binding energy and m_π is the mass of the appropriate pion. Neglecting the binding energy yields a simple scale for external momenta in these reactions, $\tilde{p} \equiv \sqrt{m_\pi M_N} = 356$ MeV.

There are two frames to keep in mind: the center of mass frame (**C**), and the laboratory frame where the proton is at rest (**E** for experiment). The experiment of interest [10] is $np \to d\pi^0$ performed in the **E** frame. In this frame the invariant is expressed as $s_{\mathbf{E}} = (M_p + M_n)^2 + 2M_p T_L$, where T_L is the kinetic energy defined by $E_n = M_n + T_L$. The experiment was performed at $T_L = 279.5$ MeV, slightly above the threshold value of $T_L = 275.1$ MeV. To simplify the formalism, we use the **C** frame to do the calculation. In terms of the pion momentum, $\vec{q}$, and the deuteron mass,

M_d, we have $\sqrt{s_{\mathbf{C}}} = \sqrt{M_d^2 + \vec{q}^2} + \sqrt{m_\pi^2 + \vec{q}^2}$. It is convenient to define a dimensionless parameter η to describe how far off threshold the reaction is, $\eta = |\vec{q}|/m_\pi$. Equating the invariants, we find $\eta_{\mathbf{C}} = 0.169$ ($q_{\mathbf{C}} = 22.86$ MeV) at the experimental energy.

We use the hybrid approach developed by Park *et al.* [15] to calculate the cross section because the initial and final states are strongly interacting. The "operator" is calculated as the sum of two-particle-irreducible diagrams involving four nucleon lines (two incoming and two outgoing) and one pion line. Then, a phenomenological potential is used to calculate the NN scattering wave fuctions and the deuteron bound-state wave function. Finally, the operator is convolved with the wave functions to obtain the matrix element. This method is described in detail in Sec. III, but first we present the selection rules for $np \to d\pi^0$.

The deuteron has the following quantum numbers: spin $S = 1$, orbital angular momentum $L = 0, 2$ (parity even), total angular momentum $J = 1$, and isospin $T = 0$. If the pion ($J^\pi = 0^-$) is produced in the s wave, then conservation of total angular momentum gives $J_i = 1$. Furthermore, because the pion is parity odd, s-wave pions must be produced from a parity odd np wavefunction, $L_i = 1$. Likewise, if the pion comes in the p wave, the initial parity is even and $J_i = 0, 1, 2$.

To completely pin down the quantum numbers of the initial state, we turn to isospin. If isospin is conserved in the final state, then $T_f = 1$ because the deuteron is an isoscalar. "Strong" diagrams have $T_i = 1$ with the isospin part of the initial wave function symmetric under exchange of nucleons. Overall wave function antisymmetry then requires $S_i = 1$ for $l_\pi = 0$ and $S_i = 0$ for $l_\pi = 1$. Thus, the initial np pair must be in the ${}^3P_1$ channel for $l_\pi = 0$, and the available channels become ${}^1S_0$ and ${}^1D_2$ for $l_\pi = 1$. CSB operators transform as vectors under isospin; thus, the initial neutron-proton state must have $T_i = 0$. The same arguments as for the strong operators then show that s-wave pions are produced from ${}^1P_1$ np pairs and p-wave pions are produced from the coupled channels ${}^3S_1$ and ${}^3D_1$ in addition to ${}^3D_2$. These conclusions are summarized in Table I.

The observable of interest in the experiment is the forward/backward asymmetry in the differential cross-section given by

$$A_{\text{fb}} = \frac{\int_0^{\pi/2} d\Omega\, [\sigma(\theta) - \sigma(\pi - \theta)]}{\int_0^{\pi} d\Omega\, \sigma(\theta)}. \tag{1}$$

A nonzero asymmetry will be observed only when initial states of opposite parity interfere. However, the interference can occur only for states with the same spin because the spin z components get summed over. Thus, for calculating the asymmetry, we are concerned with two terms: (s-wave strong)·(p-wave CSB) and (p-wave strong)·(s-wave CSB).

TABLE I. Channels for the np wave function in $np \to d\pi^0$.

	Strong	CSB
$l_\pi = 0$	${}^3P_1$	${}^1P_1$
$l_\pi = 1$	${}^1S_0, {}^1D_2$	${}^3S_1, {}^3D_1, {}^3D_2$

III. CROSS SECTION

A. Cross-section formalism

We will now derive an expression for the cross section in the **C** frame where the pion momentum is $\vec{q}$. First we must define expressions for the strongly interacting initial and final states. To form an interacting NN state with total momentum $\vec{P} = \vec{p}_1 + \vec{p}_2$, we use a superposition of free particle states,

$$\begin{aligned}|\psi(\vec{P})\rangle &= \int \frac{d^3p_1}{(2\pi)^3}\frac{d^3p_2}{(2\pi)^3}\,\psi\left(\frac{|\vec{p}_1 - \vec{p}_2|}{2}\right) \\ &\quad \times |N(\vec{p}_1), N(\vec{p}_2)\rangle \delta(\vec{P} - \vec{p}_1 - \vec{p}_2) \\ &= \int \frac{d^3p}{(2\pi)^3}\psi(p)|N(\vec{p} + \vec{P}/2), N(-\vec{p} + \vec{P}/2)\rangle, \end{aligned} \tag{2}$$

where spin and isospin have been ignored for now. The wave function $\psi(p)$ is obtained by solving the Schrödinger equation with the appropriate NN potential specified later in this article. In the **C** frame, $\vec{P}_i = 0$ and if the nucleons forming the deuteron have momentum $\vec{k}_{1,2}$, then $\vec{k}_1 + \vec{k}_2 \equiv \vec{K} = -\vec{q}$. The invariant matrix element is then

$$\begin{aligned}&\mathcal{M}[N(p_1), N(p_2) \to \pi(q), d(K)] \\ &\qquad = \int \frac{d^3k}{(2\pi)^3}\frac{d^3p}{(2\pi)^3}\,\psi_d^*(k) \\ &\qquad\quad \times \hat{\mathcal{M}}(p, k, q)\,\psi_{np}(p), \end{aligned} \tag{3}$$

where $p_{1,2} = (E_{1,2}, \pm\vec{p})$, $q = (\omega_q, \vec{q})$, and $K = (E_d, -\vec{q})$. Note that we are treating the initial state as two separate particles, but the deuteron as a single particle. As mentioned in Sec. II, the sum of the two-particle-irreducible diagrams with external momenta $\vec{q}$, $\vec{p}_{1,2}$, and $\vec{k}_{1,2}$ (the "operator") is denoted $\hat{\mathcal{M}}$, and is convolved with the external wave functions. The operator is calculated in momentum space and is a function of the external momenta p, k, and q. Also note that the wave functions will include spin and isospin wave function on which the operator acts.

We perform the calculation in position space by inserting Fourier representations of both wave functions

$$\psi_{NN}(\vec{r}) = \int \frac{d^3p}{(2\pi)^3}\, e^{i\vec{p}\cdot\vec{r}}\psi_{NN}(\vec{p}). \tag{4}$$

A Fourier representation of the operator with respect to $\vec{l} \equiv \vec{k} - \vec{p}$ is also inserted

$$\hat{\mathcal{M}}(\vec{r}) = \int \frac{d^3l}{(2\pi)^3}\, e^{i\vec{l}\cdot\vec{r}}\hat{\mathcal{M}}(\vec{l}, \vec{q}). \tag{5}$$

As described in Appendix C, $\vec{l}$ is the momentum that appears in pion production reactions: $\mathcal{M}(\vec{p}, \vec{k}, \vec{q}) \to \mathcal{M}(\vec{l}, \vec{q})$.

Now we can rewrite Eq. (3),

$$\begin{aligned}\mathcal{M} &= \int d^3r\, d^3r'\, d^3r''\, \psi_d^*(r'')\,\hat{\mathcal{M}}(\vec{r})\,\psi_{np}(r') \\ &\quad \times \int \frac{d^3k}{(2\pi)^3}\frac{d^3p}{(2\pi)^3}\, e^{i\vec{k}\cdot\vec{r}''}e^{-i(\vec{k}-\vec{p})\cdot\vec{r}}e^{-i\vec{p}\cdot\vec{r}'} \\ &= \int d^3r\, \psi_d^*(r)\,\hat{\mathcal{M}}(\vec{r})\,\psi_{np}(r). \end{aligned} \tag{6}$$

With these choices of Fourier representations, the momentum integrals evaluate to δ functions which allow evaluation of the spatial integrals. The result is an integral over a single spatial variable.

Next, we express the invariant S-matrix element in terms of $\mathcal{M}$

$$\langle \pi^0(q) d(K)|S|p(p_1), n(p_2)\rangle = 1 - i(2\pi)^4\delta^4(q + K - p_1 - p_2)\mathcal{M}(p_1, p_2 \to q, K). \tag{7}$$

In the center-of-mass frame, the differential cross section is

$$d\sigma = \frac{1}{4|\vec{p}|\sqrt{s}}\frac{1}{4}\sum_{m_d,m_1,m_2}|\mathcal{M}|^2(2\pi)^4\delta^4(q + K - p_1 - p_2) \times \frac{d^3q}{(2\pi)^3 2\omega_q}\frac{d^3K}{(2\pi)^3 2E_d}, \tag{8}$$

where we have averaged over the four np spin states and summed over the three spin states of the deuteron. The vector part of the δ function tells us $\vec{q} = -\vec{K}$ and the energy part tells us $E_1 + E_2 = \omega_q + E_d$. This allows us to perform all but the $d\Omega_K$ integral,

$$\frac{d\sigma}{d\Omega} = \frac{|\vec{q}|}{64\pi^2 s|\vec{p}|}\frac{1}{4}\sum_{m_d,m_1,m_2}|\mathcal{M}|^2. \tag{9}$$

What remains is to derive expressions for the wave functions and the operator appearing in Eq. (6).

B. Initial and final states

In the absence of interactions, the wave function $\psi_{np}(\vec{r})$ is determined by performing a partial wave expansion on an antisymmetrized wave function of a free proton and a free neutron with relative momentum $\vec{p}$. First we consider the strong operators where the np pair is in an isospin-1 state,

$$\begin{aligned}(\vec{r}|\psi_{np}\rangle &= \mathcal{P}_{T=1}\frac{1}{\sqrt{2}}(e^{i\vec{p}\cdot\vec{r}}|m_1, m_2\rangle \otimes |T_{z,1}, T_{z,2}\rangle - e^{-i\vec{p}\cdot\vec{r}} \times |m_2, m_1\rangle \otimes |T_{z,2}, T_{z,1}\rangle) \\ &= \frac{1}{\sqrt{2}}(e^{i\vec{p}\cdot\vec{r}}|m_1, m_2\rangle - e^{-i\vec{p}\cdot\vec{r}}|m_2, m_1\rangle) \otimes \frac{1}{\sqrt{2}}|T = 1, T_z = 0\rangle,\end{aligned} \tag{10}$$

where $\mathcal{P}_{T=1}$ is the isospin projector. The bra $(\vec{r}|$ indicates that we are choosing a basis for space, but not for spin or isospin. Implicit in the notation is the dependence of $(\vec{r}|\psi_{np}\rangle$ on the momentum $\vec{p}$, the spin z components of the two nucleons, m_i, and the isospin z components of the two nucleons, $T_{z,i}$, with the requirement that $T_{z,1} + T_{z,2} = 0$.

The exponentials are now expanded and the presence of the strong interaction is added by changing the spherical Bessel functions, $j_L(pr) \to e^{i\delta_L}u_{L,J}(r)/pr$. The $u_{L,J}$ functions and the δ_L phase shifts are obtained by solving the Schrödinger equation with a phenomenological NN potential (we use Argonne V18 [16]). Finally, the spherical harmonics are combined with the spin kets to form states with definite total angular momentum. The notation for these states is $|(SL)J, m_J\rangle \otimes |T, T_z\rangle$. For the allowed quantum numbers, we find

$$\begin{aligned}&(\vec{r}|\psi_{np}(^{2S+1}L_J, T = 1)\rangle \\ &= 4\pi(i)^L e^{i\delta_L}\frac{u_{L,J}(r)}{pr}\langle 1/2\, m_1, 1/2\, m_2|S\, m_s\rangle \\ &\quad\times \sum_{m_i}\langle S\, m_s, L\, m_i - m_s|J\, m_i\rangle \\ &\quad\times Y^{L\,*}_{m_i - m_s}(\hat{p})(\hat{r}|(SL)J, m_i\rangle \otimes |1, 0\rangle,\end{aligned} \tag{11}$$

where $m_s = m_1 + m_2$ and the second Clebsch Gordan coefficient allows us to make the sum over $m_i = m_l + m_s$ rather than m_l. For the CSB operators, we have $T = 0\, np$ wave functions and find

$$\begin{aligned}&(\vec{r}|\psi_{np}(^{2S+1}L_J, T = 0)\rangle \\ &= \pm 4\pi(i)^L e^{i\delta_L}\frac{u_{L,J}(r)}{pr}\langle 1/2\, m_1, 1/2\, m_2|S\, m_s\rangle \\ &\quad\times \sum_{m_i}\langle J\, m_i|S\, m_s, L\, m_i - m_s\rangle \\ &\quad\times Y^{L\,*}_{m_i - m_s}(\hat{p})(\hat{r}|(SL)J, m_i\rangle \otimes |0, 0\rangle,\end{aligned} \tag{12}$$

where the $\pm$ refers to $T_{z,1} = \pm 1/2$. Similar analysis gives the final-state wave function of the deuteron as a function of its polarization, m_f,

$$\langle \psi_d(m_f)|\vec{r}) = \langle 0, 0| \otimes \left[\frac{u(r)}{r}\langle (10)1, m_f|\hat{r}) + \frac{w(r)}{r}\langle (12)1, m_f|\hat{r})\right]. \tag{13}$$

IV. STRONG CONTRIBUTION

A. Diagrammatic expansion

Before we calculate the effects of charge symmetry, we need to discuss the power counting scheme which leads to a calculation of the total cross section in agreement with experiment. HBχPT orders contributions in powers of the external momenta divided by the chiral symmetry breaking scale, which is $\sim M_N$ [11]. In this inelastic reaction, both q and $\tilde{p}$ appear as external momenta and we need to keep track of both in the power counting. We define the expansion parameter $\chi \equiv \tilde{p}/M_N = \sqrt{m_\pi/M_N} = 0.40$.

The Lagrangian is given in Appendix A. The index of a "type i" vertex is given by

$$\nu_i = d_i + \frac{f_i}{2} - 2, \tag{14}$$

where d_i is the sum of the number of derivatives, m_π's, and δ's (the ΔN mass difference), and f_i is the number of fermion fields. In standard power counting at tree level, the sum of the ν_i for each vertex in a diagram indicates the power of χ at which that diagram contributes. This rule, however, will require modification because of the relatively large value of p.

There are three two-particle-irreducible diagrams that can be drawn using the vertices from $\mathcal{L}^{(0)}$. They will be referred to as the impulse [Fig. 1(a)], rescattering [Fig. 1(b)], and Δ

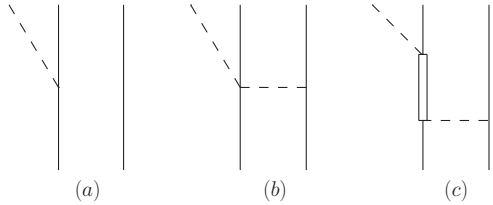

FIG. 1. Leading-order contributions to $np \to d\pi^0$. Solid lines represent nucleons, the double solid line represents a Δ, and dashed lines represent pions.

[Fig. 1(c)] diagrams. There is some ambiguity as to what is meant by Fig. 1(a). We will discuss this in detail later in this article. First let us make a few observations about these three diagrams. We have stated that the initial relative momentum is large. The final-state nucleons (the deuteron) have a comparably small relative momentum. This "momentum mismatch" is provided for in the rescattering diagram, but not in the impulse diagram. For this reason, the rescattering diagram dominates the total cross section. This diagram is strongest in the channel with s-wave pions, and the $\pi\pi NN$ vertex is typically referred to as the Weinberg-Tomozawa (WT) vertex. Next, although the Δ diagram provides the momentum transfer required, the Δ resonance is at 1232 MeV and the πN energy is $\approx$1080 MeV, so the Δ diagram is also somewhat suppressed for our situation of interest. Finally, we note that both the impulse and the Δ diagrams are strongest for the channels in which the pion is in a p wave.

We now return to the issue of the impulse diagram. On the one hand, we know that a single nucleon cannot emit a pion and remain on shell. But on the other hand, the diagrams in Fig. 2, which remedy this problem by including one pion exchange (OPE), appear to be two-particle-reducible. To resolve this issue, we first note that near threshold the energy of the exchanged pion in each of these diagrams is approximately $\omega \approx m_\pi/2$. However, the diagram of Fig. 1(a) is evaluated as diagrams of the form of Fig. 2. This is because of hybrid nature of the calculation; once the operator (traditionally, the irreducible diagram) is calculated, it is convolved with NN wave functions. One of the major terms of the strong interaction potential at low energy arises from static OPE ($\omega = 0$). We ignore the effects of the rest of the wave function for the moment. The effects of static OPE are schematically shown in Fig. 3.

To obtain the correct impulse contribution, we add up the contributions from Figs. 1(a) and 2 and then subtract what is already included in the wave functions (the two rightmost

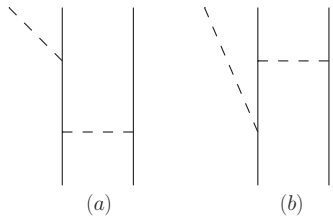

FIG. 2. Kinematically correct, but reducible impulse contributions. Solid lines represent nucleons and dashed lines represent pions.

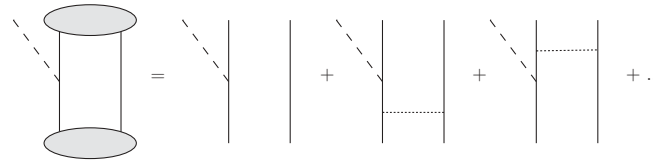

FIG. 3. "Hybrid" approach. Solid lines represent nucleons, dashed lines represent pions, dotted lines represent pions with $\omega = 0$, and shaded ovals represent NN strong interactions.

diagrams of Fig. 3). This calculation is schematically shown in Fig. 4.

The OPE propagator is of Yukawa form,

$$D_\pi(r) = -\frac{e^{-\mu(\omega)r}}{4\pi r}, \tag{15}$$

where $\mu(\omega) = \sqrt{m_\pi^2 - \omega^2} \approx \sqrt{3}/2m_\pi$. Thus, subtracting off the final two diagrams in Fig. 4 amounts to making the replacement

$$\frac{e^{-\sqrt{3}m_\pi r/2}}{r} \to \frac{e^{-\sqrt{3}m_\pi r/2}}{r} - \frac{e^{-m_\pi r}}{r} \tag{16}$$

in the exchanged pion propagator. The final four terms of Fig. 4 comprise a correction to the impulse diagram, which we will refer to as a "wave function correction." We find that this correction is $\sim$4% of the total impulse amplitude at the experimental energy, and we include it in our calculation.

B. Power counting

Now we will look more closely at the size of these diagrams in the "$\tilde{p}$ kinematics," using the counting techniques developed in Ref. [17]. The propagators are calculated from the Lagrangian in Eq. (A1):

$$\begin{aligned} D_N(p) &= \frac{i}{p^0 + i\epsilon} \\ D_\Delta(p) &= \frac{i}{p^0 - \delta + i\epsilon} \\ D_\pi(p) &= \frac{-i}{\vec{p}^2 + [m_\pi^2 - (p^0)^2] - i\epsilon}. \end{aligned} \tag{17}$$

Both the πNN and the $\pi N\Delta$ vertices have a momentum dependence of $|\vec{q}|$, the pion momentum *at that vertex*. Note that this momentum is $\tilde{p}$ in the OPE verticies. The WT vertex contains a factor of $\omega_{q,\text{in}} + \omega_{q,\text{out}}$.

The external particles have the same momenta in each diagram. The produced pion has $q = (\omega_q, \vec{q}) \approx (m_\pi, 0)$, and the incoming nucleons have $p_{1,2} = (E_{1,2}, \pm\vec{p}) \approx (m_\pi/2, \pm\vec{\tilde{p}})$ in the heavy baryon formalism in which the nucleon mass is subtracted off of the energy component. Consider the impulse diagram of Fig. 2(a). The final emission contributes q, the nucleon propagator $1/m_\pi$, and the OPE $\tilde{p} \cdot 1/\tilde{p}^2 \cdot \tilde{p}$, so that the diagram is $\sim q/m_\pi = \eta$. The rescattering diagram is $\sim \frac{3m_\pi/2}{\tilde{p}} \sim \chi$, and the Δ diagram is $\sim \frac{q}{m_\pi - \delta}$. Finally, note that $\eta \approx \chi^2$ and $\delta \approx 2m_\pi$ so that though the rescattering diagram is $\sim \chi$ the impulse and Δ diagrams are numerically $\sim\chi^2$. This ordering comes in agreement with the fact that the rescattering

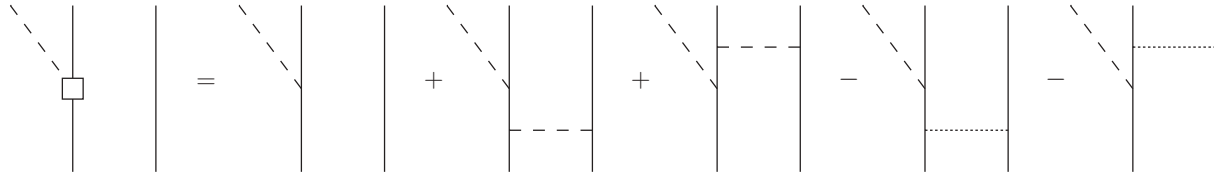

FIG. 4. Complete impulse contribution. Solid lines represent nucleons, dashed lines represent pions, dotted lines represent "wave function" pions with $\omega = 0$, and the square represents the operator that is used for the full impulse approximation.

diagram is strongest for s-wave pions and the impulse and Δ diagrams are strongest for p-wave pions.

It is well documented that these three diagrams alone do not correctly reproduce the experimental data for the reaction; see Ref. [17] for a review of the theory of meson production. Near threshold ($\eta \approx 0.05$), the most recent experiment found $\alpha_{\rm exp}(np \to d\pi^0) \approx 90\ \mu$b [18], and for these first three diagrams, we find $\alpha \approx 55\ \mu$b. The solution to this problem was discovered by the authors of Ref. [11], who noticed that the $\nu = 1$ "recoil" correction to the WT vertex, which is found in Eq. (A2), goes like $(\vec{q}_{\rm in} + \vec{q}_{\rm out}) \cdot (\vec{p}_{\rm in} + \vec{p}_{\rm out})/(2M_N)$, where $\vec{q}$ is the pion momentum and $\vec{p}$ is the nucleon momentum. For Fig. 5(a), this vertex (a solid circle) $\sim \vec{p}^{\,2}/(2M_N) = m_\pi/2$ and thus this diagram is of order χ, the same order as the $\nu = 0$ rescattering diagram. Similarly, one finds that the s-wave portion of the recoil correction to the impulse diagram [Fig. 5(b)] is of order χ. In this diagram, the solid square represents the sum analogous to Fig. 4 for the recoil diagram. We find that the wave function corrections are more important ($\sim$20%) in this case. Finally, the s-wave portion of the Δ diagram's recoil correction is found to be higher order and is therefore ignored.

The recoil corrections to the propagators have also been included in the calculation where applicable. For this reaction, the only such diagram is Fig. 2(b), where the three-momentum in the nucleon propagator is large ($\sim\tilde{p}$). For that propagator, we use the corrected version,

$$D_N(p) = \frac{i}{p^0 - \vec{p}^{\,2}/2M_N + i\epsilon} \approx -\frac{i}{m_\pi}. \qquad (18)$$

Using this propagator rather than the $\nu = 0$ version doubles the size of Fig. 2(b). Nevertheless, this diagram (minus its $\omega_\pi = 0$ analog) is already very small. Thus, the net effect of correcting the propagators is small for this reaction at this order.

Including all these recoil corrections [especially Fig. 5(a)] brings the theoretical cross section near the experimental results as shown by the solid curve in Fig. 6 [18]. Because of the relative scatter of the data shown in Fig. 6, it is difficult to tell how well the theory is reproducing the experiment. Regardless, it is clear that theoretical improvement has been made.

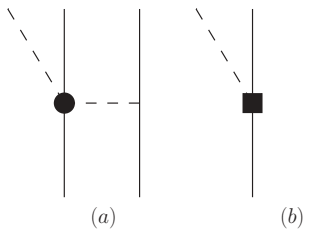

FIG. 5. Recoil corrections. Solid lines represent nucleons, dashed lines represent pions, and the solid circle and square represent $\nu = 1$ vertices.

It should also be noted that the subtlety of reducibility and recoil corrections in this reaction resolves questions about next-to-leading-order (NLO) loop diagrams discovered by the authors of Ref. [19]. Namely, the sum of all the NLO irreducible loops in Fig. 7 is found to be proportional to $\vec{p}$. This is a problem because such sensitivity of the operator to the NN wave function is not physical. Again, one considers including OPE in the operator, this time for the rescattering diagram. There are two resulting diagrams shown in Fig. 8. It was shown in Ref. [11] that in these reducible loops, the recoil corrections to the nucleon propagators need to be included in addition to the WT's recoil correction. Reference [11] then showed that (part of) the energy dependence of the WT vertex "cancels" one of the nucleon propagators, leaving a reducible diagram similar to Fig. 7(a). This diagram is equal in magnitude and opposite in sign to the aforementioned NLO sum, resolving the issue. The other term that remains from the original loop integral after this manipulation is still of reducible form but now has an on-shell WT vertex $\sim 2m_\pi$. This term would already appear upon convolution of the rescattering diagrams discussed earlier in this article (including recoil corrections) with external wave functions; that is, this term

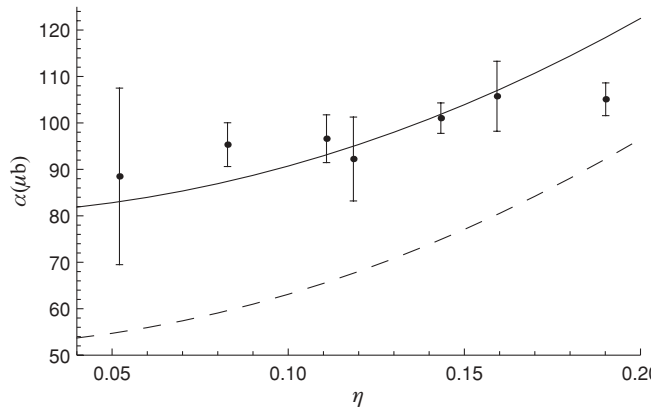

FIG. 6. Cross section for $np \to d\pi^0$ in terms of $\alpha = \sigma/\eta$ as a function of the pion center of mass momentum, $\eta = q/m_{\pi^0}$. Circles with error bars display the experimental results of Ref. [18]. The dashed line displays the results of including the diagrams in Fig. 1 and the solid line displays the results of also including the recoil terms discussed in the text.

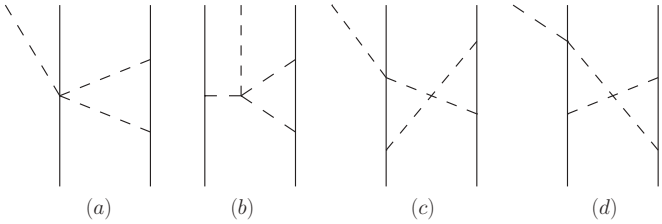

FIG. 7. Irreducible loops. Solid lines represent nucleons and dashed lines represent pions.

is truly reducible. This result can be stated another way: Cancellation of the irreducible loops comes from a short-range piece of including OPE in the rescattering operator. Thus, a complete NLO calculation must include this OPE. However, its remaining reducible piece would only be included in the calculation if the recoil correction to the WT vertex is included in the rescattering operator. Therefore, it is both consistent and necessary to include the WT recoil correction, which was shown earlier in this article to reproduce the total cross section.

C. *p*-wave observables

Another important test of the theory is how well it describes p-wave pions [20]. This is especially important for the asymmetry, which involves strong p waves at leading order. The differential cross section can be expanded in Legendre polynomials,

$$\frac{d\sigma}{d\Omega} = \alpha_0 + \alpha_1 P_1[\cos(\theta)] + \alpha_2 P_2[\cos(\theta)] + \cdots, \tag{19}$$

where θ is the angle between $\vec{p}$ and $\vec{q}$. Note that the total cross section plotted in Fig. 6 is $\alpha = 4\pi\alpha_0/\eta$. As discussed in Appendix D, α_2 receives contributions almost exclusively from p-wave pions. The ratio α_2/α_0 is therefore used as a test for this part of the theory. We find that the diagrams of Fig. 1 along with their recoil corrections overestimate the data by approximately a factor of two. Upon closer inspection, we find that the $^1S_0$ amplitude (which is known to be small) is relatively large. This amplitude is coming mainly from the Δ diagram, as can be seen in Appendix D, where the values of the reduced matrix elements are listed. To remedy the situation in the simplest way possible, we implement a cutoff for the

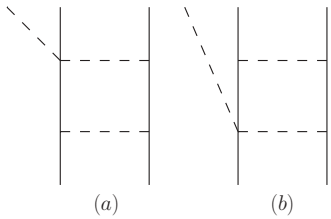

FIG. 8. Reducible loops. Solid lines represent nucleons and dashed lines represent pions.

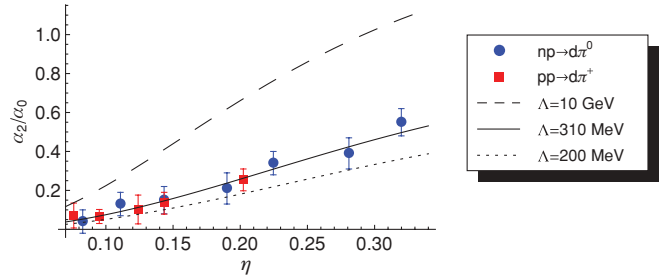

FIG. 9. (Color online) Legendre coefficients of the differential cross section for different values of the cutoff. Data are from an $np \to d\pi^0$ experiment (Ref. [18], circles) and an $\vec{p}p \to d\pi^+$ experiment (Ref. [22], squares) in which the data have not been corrected for Coulomb effects.

Δ diagram,

$$D_\pi = \frac{-i}{\vec{p}^2 + \mu^2} \to D_\pi^c(\Lambda) \equiv \frac{-i}{\vec{p}^2 + \mu^2}\left(\frac{\Lambda^2}{\vec{p}^2 + \Lambda^2}\right) = \left(\frac{-i}{\vec{p}^2 + \mu^2} - \frac{-i}{\vec{p}^2 + \Lambda^2}\right)\frac{\Lambda^2}{\Lambda^2 - \mu^2}. \tag{20}$$

One can show that doing this essentially softens the OPE potential for $r < \log(\Lambda/\mu)/\Lambda$. Note that one consequence of such a cutoff is that it modifies both the $^1S_0$ and the $^1D_2$ channels. Clearly, this cutoff is not an acceptable long-term solution for an effective field theory, but the fact that such a procedure is necessary is interesting given that the reaction occurs at an energy ~150 MeV below the Δ resonance. That p-wave pion production is highly sensitive to the strength of its contact term was discussed in Ref. [21].

Figure 9 shows the effects of this cutoff on the ratio α_2/α_0, where $\Lambda = 10$ GeV represents the original theory (such a large cutoff has no significant effect). Note that the amplitudes for $np \to d\pi^0$ are related to those for $pp \to d\pi^+$ (which are bigger by $\sqrt{2}$) when charge symmetry is respected. Thus, the ratio plotted should have the same value for both reactions. Also note that for simplicity we used a single cutoff and that if we had used one at each vertex of the OPE we would have found $\Lambda \to \sqrt{2}\Lambda$. By adjusting the cutoff to fit the data, we find $\Lambda = 310$ MeV.

Another useful observable for testing p-wave pion production is the analyzing power, A_y, which is defined

$$A_y(\theta) \equiv \frac{d\sigma_\uparrow(\theta) - d\sigma_\downarrow(\theta)}{d\sigma_\uparrow(\theta) + d\sigma_\downarrow(\theta)} \tag{21}$$

$$d\sigma_{\uparrow,\downarrow}(\theta) \equiv \frac{|\vec{q}|}{64\pi^2 s|\vec{p}|}\frac{1}{4}\sum_{m_d,m_2} |\mathcal{M}(m_{1,y} = \pm 1/2, \theta)|^2, \tag{22}$$

where $m_{1,y} = \pm 1/2$ refers to the fact that the beam is polarized perpendicular to the scattering plane. In the z basis, these states are

$$\mathcal{M}(m_{1,y} = \pm 1/2) = \frac{\mathcal{M}(m_1 = 1/2) \pm i\mathcal{M}(m_1 = -1/2)}{\sqrt{2}}. \tag{23}$$

As shown in Appendix D, A_y is proportional to the product of s-wave and p-wave amplitudes. Figure 10 shows the effects of

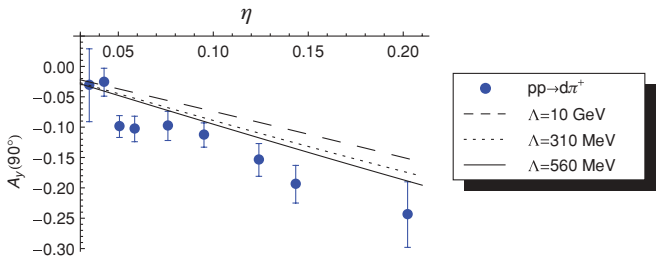

FIG. 10. (Color online) Analyzing power for different values of the cutoff. Data are from a $\vec{p}p \to d\pi^+$ experiment (Ref. [22], circles) in which the data have not been corrected for Coulomb effects.

the cutoff on this observable. Again, charge symmetry implies that A_y should be the same for both neutral and charged pion production. We find the best agreement with the data for $\Lambda = 560$ MeV. Later in this article, we will display our results using both the original theory and a cutoff taken to be the geometric mean of two fits, $\Lambda = 417$ MeV.

V. CHARGE SYMMETRY BREAKING

The fact that the up and down quarks have different mass is reflected in the Lagrangian by including terms that break chiral symmetry [23]. The leading such terms are given in Eq. (A2) and have coupling constants δm_N and $\bar{\delta} m_n$ which are constrained by

$$\delta m_N + \bar{\delta} m_N = M_n - M_p. \tag{24}$$

The δm_N term has its origins in the quark mass difference and its size is $\sim(m_d - m_u) \equiv \epsilon(m_d + m_u)$, with $\epsilon \approx 1/3$. The formalism of χPT tells us that $(m_d + m_u) \propto m_\pi^2$, and so dimensional analysis along with the natural QCD scale, M_N, yields $\delta m_N \sim \epsilon m_\pi^2 / M_N$. The $\bar{\delta} m_N$ term is of electromagnetic origins, but is of the same order as δm_N. These CSB operators appear in the rescattering diagram depicted in Fig. 11. where the CSB vertex is denoted with a cross. The size of this diagram is $\delta m_N / \tilde{p} \approx \epsilon m_\pi^2 / (M_N \tilde{p}) = \epsilon \chi^3$. Note that although the full nucleon mass difference appears explicitly in the Lagrangian at this order, the corresponding operator $(N^\dagger \tau_3 N)$ does not change the parity and thus does not contribute to an asymmetry. In Sec. VII, we will discuss another source of CSB coming from a more detailed evaluation of the diagram of Fig. 1(b) that was made in Ref. [14].

Another CSB term given in Eq. (A3) involves one derivative and one m_π^2 ($\beta_1 \sim \epsilon m_\pi^2 / M_N^2$) and is thus a $\nu = 2$ vertex

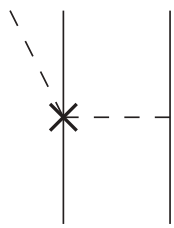

FIG. 11. Leading CSB contribution. Solid lines represent nucleons, dashed lines represent pions, and the cross represents the $\nu = 1$ CSB vertex.

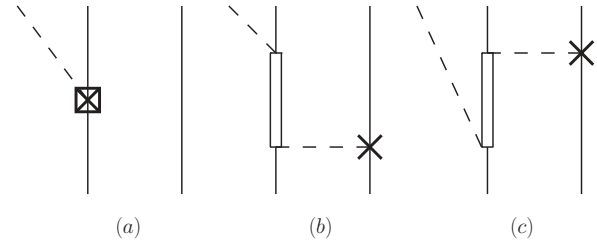

FIG. 12. $\nu = 2$ CSB contributions. Solid lines represent nucleons, double solid lines represent Δ's, dashed lines represent pions, crosses represent $\nu = 2$ CSB vertices, and the boxed cross represents the full impulse CSB diagram including OPE.

with momentum dependence $|\vec{q}|$. This vertex appears in the diagrams of Fig. 12, whose sizes are $\beta_1 q / m_\pi \approx \epsilon \eta \chi^4$. In Fig. 12(a), the boxed cross represents the sum analogous to Fig. 4 for the CSB impulse diagram. Again, the wave function corrections are small (2%).

As mentioned in Sec. II, contributions to the asymmetry come from interference terms between the p-wave part of the strong amplitude and the s-wave part of the CSB amplitude, and vice versa. The issue is somewhat complicated because, in contrast to threshold emission, each diagram can contribute in both the s wave and the p wave. However, contributions to the subleading parity (s wave for the impulse and Δ diagrams and p wave for the rescattering diagrams) are formally higher order. For example, the strong rescattering diagram for p-wave pions comes with an m_π from the WT vertex, a $1/\tilde{p}^2$ from the pion propagator, and a q from the pion emission in the p wave. Thus, the diagram counts as $\sim \eta \chi^2$. The contributions to the asymmetry are depicted in Fig. 13. Figure 13(a) includes strong p waves and CSB s waves and has size $(\eta) \times (\epsilon \chi^3)$. Figure 13(b) includes strong s waves and CSB p waves and has size $(\chi) \times (\epsilon \eta \chi^4)$. Figure 13(c) includes strong p waves and CSB s waves and has size $(\eta \chi^2) \times (\epsilon \chi^3)$. Thus, we find that in these kinematics Fig. 13(a) ($\sim \epsilon \eta \chi^3$) is the leading-order (LO) contribution, and Figs. 13(b) and 13(c) ($\sim \epsilon \eta \chi^5$) both come in at NLO. Other interference terms involving these diagrams are higher order, $\sim \epsilon \eta^3 \chi^5$ or smaller. Finally, we note that this work is not intended to be a complete NLO calculation as loops and higher-order vertices may come in at NLO.

VI. CSB RESULTS

In this section we discuss the CSB results of our calculation. The coupling of the WT vertex (and its recoil correction) is determined by chiral symmetry and we use $f_\pi = 91.9$ MeV. For the impulse vertices we use the values $g_A = 1.267$ and $h_A = 2.1 g_A$. We use the following masses: $M_N = (M_n + M_p)/2 = 938.919$ MeV, $M_n - M_p = 1.293$ MeV, $M_\Delta = 1232$ MeV, and $m_\pi = m_{\pi^0} = 134.977$ MeV. Consider now the CSB coupling constants. The Cottingham formula can be used to obtain $\bar{\delta} m_N = -(0.76 \pm 0.30)$ MeV [24]. The constraint of Eq. (24) then fixes $\delta m_N = 2.05 \pm 0.30$ MeV. The combination of these parameters that appears in the asymmetry is $\delta m_N - \bar{\delta} m_N / 2 = 2.4 \pm 0.3$ MeV. It is also noted in Ref. [13] that other models predict different values for $\bar{\delta} m_N$ leading to $1.83 \leqslant \frac{\delta m_N}{\text{MeV}} \leqslant 2.83$.

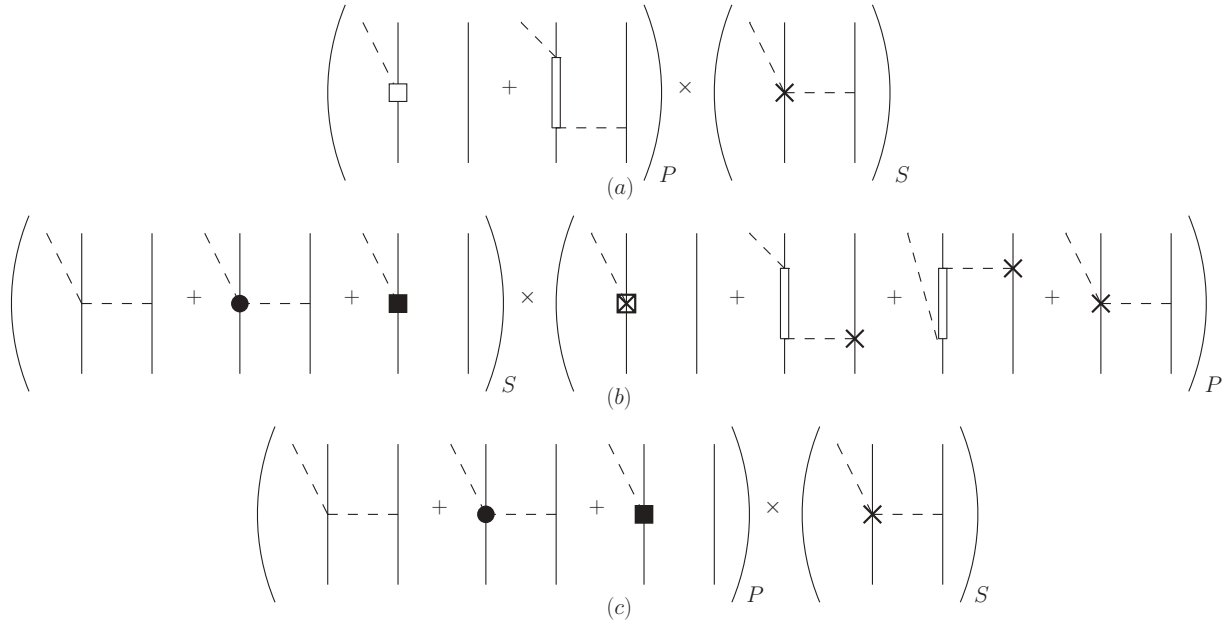

FIG. 13. Interference terms for the asymmetry in $np \to d\pi^0$. Solid lines represent nucleons, double solid lines represent Δ's, and dashed lines represent pions. The solid circle and square represent $\nu = 1$ strong vertices and the crosses represent CSB vertices. The boxes represent full impulse diagrams in the sense of Fig. 4.

Even less is known about β_1, the impulse CSB coupling. As a starting point, Ref. [25] notes that this CSB operator can be viewed as arising from π-η mixing. The result shown is that

$$\beta_1 = \frac{g_\eta f_\pi}{M_N m_\eta^2}\langle\pi^0|H|\eta\rangle = c_\eta\left(\frac{\epsilon\, m_\pi^2}{M_N^2}\right). \tag{25}$$

As discussed in the review [7],

$$0.10 \leqslant \frac{g_\eta^2}{4\pi} \leqslant 0.51. \tag{26}$$

Also, Ref. [26] gives $\langle\pi^0|H|\eta\rangle = -0.0039\ \text{GeV}^2$, and we use $m_\eta = 547.51$ MeV. These values result in $-0.47 \leqslant c_\eta \leqslant -0.21$. Thus, it is at least plausible that the β_1 term could originate naturally from η-π mixing. We note that the η' could also give such a term, but do not consider it here. Using Eqs. (25) and (26), we obtain $-3.2 \times 10^{-3} \leqslant \beta_1 \leqslant -1.4 \times 10^{-3}$. Note that the value used in the original calculation of the asymmetry in Ref. [12] was $\beta_1 = -8.7 \times 10^{-3}$, which we refer to as the "extreme value." However, recall from the above discussion that the natural size of the p-wave CSB is $\beta_1 \sim -\frac{\epsilon m_\pi^2}{M_N^2} \approx -6 \times 10^{-3}$. Thus, even though its origins may not lie exclusively with the η, the aforementioned "extreme" value for β_1 is not extreme at all from the effective field theory's point of view.

In Table II, we display our results which are obtained by using Eq. (24) to eliminate $\bar{\delta}m_N$ so that the diagram of Fig. 11 is proportional to

$$\delta m_N - \frac{\bar{\delta}m_N}{2} = \frac{3\delta m_N}{2} - \frac{M_n - M_p}{2}. \tag{27}$$

Because the asymmetry is linear in the CSB amplitudes (and therefore the CSB parameters), we are able to present our results as a set of coefficients, $\{x, y, z\}$ defined by

$$A_{fb} \times 10^4 = x \cdot \left(\frac{\delta m_N}{\text{MeV}}\right) + y \cdot (\beta_1 \times 10^3) + z. \tag{28}$$

The primary advance made in this work over the the previous calculation of Ref. [13] (including the rescattering and impulse recoil corrections) is shown in moving from the top four rows to the next four rows. At LO this simply increases α_0, but at NLO it affects both the numerator and the denominator of the asymmetry.

The experiment of Ref. [10] found $A_{\text{fb}} = [17.2 \pm 9.7] \times 10^{-4}$. The first calculation of the asymmetry used an $N\Delta$ coupled-channel formalism and included the CSB impulse vertex as well as other, smaller effects arising directly from the neutron-proton mass difference [12]. This study reported $A_{\text{fb}} = -28 \times 10^{-4}$. The second calculation included only the CSB rescattering vertex and found $A_{\text{fb}} = 60 \times 10^{-4}$ [13]. Both these calculations were preformed before the work of Ref. [11], which brought the total cross section into agreement with experiment. Our work brings the asymmetry calculation up to date.

As shown in Table II, the value of A_{fb} is overpredicted for the set of physically reasonable parameters used in the last column. Nevertheless, for the most "extreme" set of parameters discussed above ($\delta m_N = 1.83$ MeV, $\beta_1 = -8.7 \times 10^{-3}$) the cutoff NLO calculation yields $A_{\text{fb}} = 16.9 \times 10^{-4}$. The effects of using different values for the cutoff can be seen in the last two rows of the table. Because of the large number of theoretical issues that still need to be addressed, we refrain from providing an uncertainty at this time.

TABLE II. Asymmetry in $np \to d\pi^0$ as a function of CSB parameters δm_N and β_1. "LO" and "NLO" represent the sums discussed in Fig. 13. The term z arises from the influence of the term proportional to $\frac{M_n - M_p}{2}$.

	$A_{\rm fb} \times 10^4 = x \cdot (\frac{\delta m_N}{\rm Mev}) + y \cdot (\beta_1 \times 10^3) + z$				$A_{\rm fb}(\delta m_N = 2.05$ MeV, $\beta_1 = -3.2 \times 10^{-3}) \times 10^4$
Order	Δ cutoff	x	y	z	
LO (no recoil)	None	33.7	0	−14.5	54.6
LO (no recoil)	$\Lambda = 417$ MeV	27.6	0	−11.9	44.7
NLO (no recoil)	None	37.6	1.4	−16.2	56.4
NLO (no recoil)	$\Lambda = 417$ MeV	32.5	1.8	−14.0	47.0
LO	None	25.0	0	−10.8	40.4
LO	$\Lambda = 417$ MeV	18.9	0	−8.2	30.7
NLO	None	28.1	1.4	−12.1	41.0
NLO	$\Lambda = 417$ MeV	22.1	1.6	−9.5	30.7
NLO	$\Lambda = 310$ MeV	20.1	1.7	−8.7	27.3
NLO	$\Lambda = 560$ MeV	24.0	1.6	−10.4	33.9

VII. DISCUSSION

We have mentioned that it is difficult to tell how well the current theory is reproducing the total cross section. We have also seen that there is reason for concern regarding the theoretical description of p-wave pions, which comprise the entire strong contribution to the LO asymmetry. Because the total cross section is dominated by the rescattering diagram, small changes to the p-wave amplitudes are able to significantly modify the asymmetry while only slightly changing the total cross section. As a temporary solution, we implemented a cutoff in the Δ diagram and thereby achieved acceptable agreement with the p-wave data. Another solution to this problem is to use a coupled-channel $N\Delta$ potential for the initial state. This approach was taken by the authors of Ref. [14], who were able to achieve good fits to these data without a cutoff, because the OPE of the Δ diagram is then part of the wave function.

There are other significant differences between Ref. [14] and this work. First of all, the authors of that article discovered an additional CSB contribution to the asymmetry which is a consequence of the time derivative in the WT vertex. The effect of this contribution is equivalent to a change in the CSB rescattering diagram,

$$\frac{3\delta m_N}{2} - \frac{M_n - M_p}{2} \to \frac{3\delta m_N}{2}. \tag{29}$$

Thus, to update our calculation, we drop the fifth column of Table II (the z column). Second, to improve on the theoretical uncertainty ($\sim$30%) of the Legendre coefficient α_0, they used experimental data (from pionic deuterium) to obtain $\alpha_0 = 1.93$ μb. This is significantly larger than the theoretical value we use, $\alpha_0 = 1.49$ μb at LO ($\alpha_0 = 1.28$ μb for $\Lambda = 417$ MeV), and leads to a smaller value for the for the asymmetry. Note that experiments for neutral [18] and charged [22] pion production found $\alpha_0 = 1.39$ μb and $\alpha_0 = 1.64$ μb (Coulomb corrected), respectively. Finally, they do not include the NLO CSB diagrams.

For the sake of comparison, we used our code to calculate the LO asymmetry with $\Lambda = 417$ MeV, without the z column, using $\alpha_0 = 1.93$, and using their quoted values for g_A and f_π. For these choices we obtain $A_{\rm fb} = 14.0 \frac{\delta m_N}{\rm MeV} \times 10^{-4}$, which is to be compared with their result of $A_{\rm fb} = 11.5 \frac{\delta m_N}{\rm MeV} \times 10^{-4}$. Using the Cottingham sum rule, along with their result, one obtains $\delta m_N = 2.0$ MeV and thus $A_{\rm fb} = 23 \times 10^{-4}$, which only overestimates the data by 0.6σ. Finally, we display our best result without the z column,

$$A_{\rm fb} = 22.1 \frac{\delta m_N}{\rm MeV} + 1.6(\beta_1 \times 10^3). \tag{30}$$

For the set of parameters used in Table II, $A_{\rm fb} = 40.2 \times 10^{-4}$, which is an overestimation of the data by 2.4σ.

Several issues remain to be understood theoretically. First, it appears that a large contact term will be required to suppress the ${}^1S_0$ channel in the strong amplitude if one uses a purely NN initial state. The interesting physics observation here is that the Δ part of the NN wave function seems to be much more active than it is NN scattering. Second, the difference between the more recent experimental determination of α_0 (from pionic deuterium) and the older $np \to d\pi^0$ data (which agrees with NLO theory) may play a large role in the overprediction of our calculation. This situation becomes even worse when a cutoff is used to decrease the p-wave amplitudes. For these reasons, we conclude that further calculations are necessary. In particular, one should extend the calculation to next order while examining both the power counting of recoil terms and the reducibility of loops.

More generally, the existence of multiple mass scales greatly complicates the power counting for this reaction, and it is clear that a converging expansion cannot yet be definitively claimed. Another interesting aspect of this calculation is the use of a hybrid formalism. One can argue that using phenomenological potentials to determine the NN wave functions is equivalent to working to all orders in the EFT. Thus, there is a mismatch when the calculation of the operator is truncated at some order. One way to remedy this situation (introduced by [27]) is to use a cutoff when calculating the Fourier transforms of the operators. Indeed, such a study for pion production would be interesting.

ACKNOWLEDGMENTS

We thank U. van Kolck, D. Phillips, and the authors of Ref. [14] for useful discussions. This research was supported in part by the US Department of Energy.

APPENDIX A: LAGRANGE DENSITIES

The $\nu = 0$ Lagrangian of HBχPT (with isovectors in **bold** font) with the Δ included as an explicit degree of freedom is [28]

$$\begin{aligned}\mathcal{L}^{(0)} &= \frac{1}{2}(\partial\boldsymbol{\pi})^2 - \frac{1}{2}m_\pi^2\boldsymbol{\pi}^2 + N^\dagger i\partial_0 N \\ &\quad - \frac{1}{4f_\pi^2}N^\dagger[\boldsymbol{\tau}\cdot(\boldsymbol{\pi}\times\dot{\boldsymbol{\pi}})]N + \frac{g_A}{2f_\pi}N^\dagger(\boldsymbol{\tau}\cdot\vec{\sigma}\cdot\vec{\nabla}\boldsymbol{\pi})N \\ &\quad + \Delta^\dagger(i\partial_0 - \delta)\Delta + \frac{h_A}{2f_\pi} \\ &\quad \times [N^\dagger(\mathbf{T}\cdot\vec{S}\cdot\vec{\nabla}\boldsymbol{\pi})\Delta + \text{H.c.}] + \cdots, \end{aligned} \tag{A1}$$

where $\mathbf{T}$ and $\vec{S}$ are the $3/2 \to 1/2$ isospin and spin transition operators, and $\boldsymbol{\tau}$ and $\vec{\sigma}$ are the Pauli matrices acting on the isospin and spin of a single nucleon. The "$+\cdots$" indicates that only the terms used in this calculation are shown.

The $\nu = 1$ Lagrangian includes propagator corrections, recoil terms, and the leading s-wave CSB operator,

$$\begin{aligned}\mathcal{L}^{(1)} &= \frac{1}{2m_N}N^\dagger\nabla^2 N + \frac{1}{2m_N}\left[\frac{1}{4f_\pi^2}iN^\dagger\boldsymbol{\tau}\cdot(\boldsymbol{\pi}\times\vec{\nabla}\boldsymbol{\pi})\cdot\vec{\nabla}N\right. \\ &\quad \left. - \frac{g_A}{2f_\pi}iN^\dagger\boldsymbol{\tau}\cdot\dot{\boldsymbol{\pi}}\vec{\sigma}\cdot\vec{\nabla}N + \text{H.c.}\right] \\ &\quad + \frac{1}{2m_N}\Delta^\dagger\nabla^2\Delta - \frac{1}{2m_N}\frac{2h_A}{2f_\pi}(iN^\dagger\mathbf{T}\cdot\dot{\boldsymbol{\pi}}\vec{S}\cdot\vec{\nabla}\Delta + \text{H.c.}) \\ &\quad + \frac{\delta m_N}{2}N^\dagger\left(\tau_3 - \frac{2}{4f_\pi^2}\pi_3\boldsymbol{\tau}\cdot\boldsymbol{\pi}\right)N + \frac{\bar{\delta}m_N}{2}N^\dagger \\ &\quad \times\left[\tau_3 + \frac{2}{4f_\pi^2}\left(\pi_3\boldsymbol{\tau}\cdot\boldsymbol{\pi} - \tau_3\boldsymbol{\pi}^2\right)\right]N + \cdots. \end{aligned} \tag{A2}$$

Although there are a host of $\nu = 2$ terms, we list the just the CSB term relevant for this calculation

$$\mathcal{L}^{(2)} = \frac{\beta_1}{2f_\pi}N^\dagger\vec{\sigma}\cdot\vec{\nabla}\pi_3 N + \cdots. \tag{A3}$$

APPENDIX B: DEFINING REDUCED MATRIX ELEMENTS

One can show that for s-wave pions the production operator is always either a scalar or a rank-two tensor and for p-wave pions it is always a rank-one tensor. This guides the following definition of the reduced matrix elements. Note that the Clebsch-Gordan coefficients that will be summed over as well as the spherical harmonics describing the angular distribution of the differential cross section are "pulled out." First we define the strong reduced matrix elements,

$$\begin{aligned}\langle f|\hat{\mathcal{M}}^{\text{str}}_{l_\pi=0}|i\rangle &= \left(\frac{1}{\sqrt{3}}A_0 + \frac{\langle 1m_f, 20|1m_f\rangle}{\sqrt{3}}A_2\right)e^{i\delta_1}\text{cg}_1 \\ &\quad \times\langle 1m_s, 1m_f - m_s|1m_f\rangle Y^{1*}_{m_f-m_s}(\hat{p}) \end{aligned} \tag{B1}$$

$$\begin{aligned}\langle f|\hat{\mathcal{M}}^{\text{str}}_{l_\pi=1}|i\rangle &= \frac{1}{\sqrt{3}}Be^{i\delta_0}\text{cg}_0\delta_{m_f,0}Y^0_0(\hat{p}) \\ &\quad + \frac{\langle 2m_f, 10|1m_f\rangle}{\sqrt{3}}Ce^{i\delta_2}\text{cg}_0 Y^{2*}_{m_f}(\hat{p}), \end{aligned} \tag{B2}$$

where $m_s = m_1 + m_2$, $\text{cg}_0 = \langle 1/2\, m_1, 1/2\, m_2|0\, 0\rangle$, and $\text{cg}_1 = \langle 1/2 m_1, 1/2 m_2|1 m_s\rangle$. A_0 and A_2 are the s-wave reduced matrix elements, and B and C are the p-wave reduced matrix elements. To clarify the notation consider A_2, for example.

$$\begin{aligned}A_2 &= \int drr^2\left[\frac{u_d(r)}{r}\langle(10)1||\right. + \left.\frac{w_d(r)}{r}\langle(12)1||\right] \\ &\quad \times\hat{\mathcal{M}}^{\text{str}}_{l_\pi=0,J=2}\left[4\pi i\frac{u_{1,1}(r)}{pr}||(11)1\rangle\right], \end{aligned} \tag{B3}$$

where the subscript $J = 2$ on the $\hat{\mathcal{M}}$ indicates that we are using the portion of the operator that is a rank-two tensor in the space of total angular momentum. Note also that we have used the following general definition of a reduced matrix element,

$$\begin{aligned}&\langle(S'L')J'm'_J|T^k_q|(SL)Jm_J\rangle \\ &\quad \equiv \frac{\langle Jm_J, kq|J'm'_J\rangle}{\sqrt{2J'+1}}\langle(S'L')J'||T^k||(SL)J\rangle. \end{aligned} \tag{B4}$$

Similarly for the CSB reduced matrix elements,

$$\begin{aligned}&\langle f|\hat{\mathcal{M}}^{\text{csb}}_{l_\pi=0}|i\rangle \\ &\quad = \left(\frac{1}{\sqrt{3}}\overline{A}_0 + \frac{\langle 1m_f, 20|1m_f\rangle}{\sqrt{3}}\overline{A}_2\right)e^{i\bar{\delta}_1}\text{cg}_0 Y^{1*}_{m_f}(\hat{p}) \end{aligned} \tag{B5}$$

$$\begin{aligned}&\langle f|\hat{\mathcal{M}}^{\text{csb}}_{l_\pi=1}|i\rangle \\ &\quad = \frac{\langle 1m_f, 10|1m_f\rangle}{\sqrt{3}}(\overline{B}_\alpha e^{i\bar{\delta}_\alpha} + \overline{B}_\beta e^{i\bar{\delta}_\beta})\text{cg}_1\delta_{m_f,m_s}Y^0_0(\hat{p}) \\ &\quad\quad + \frac{\langle 1m_f, 10|1m_f\rangle}{\sqrt{3}}(\overline{C}_\alpha e^{i\bar{\delta}_\alpha} + \overline{C}_\beta e^{i\bar{\delta}_\beta})\text{cg}_1 \\ &\quad\quad \times\langle 1m_s, 2m_f - m_s|1m_f\rangle Y^{2*}_{m_f-m_s}(\hat{p})\frac{\langle 2m_f, 10|1m_f\rangle}{\sqrt{3}} \\ &\quad\quad \times\overline{D}e^{i\bar{\delta}_2}\text{cg}_1\langle 1m_s, 2m_f - m_s|2m_f\rangle Y^{2*}_{m_f-m_s}(\hat{p}), \end{aligned} \tag{B6}$$

where $\overline{A}_0$ and $\overline{A}_2$ are the s-wave reduced matrix elements and $\overline{B}$, $\overline{C}$, and $\overline{D}$ are the p-wave reduced matrix elements. Also note that the strong phase shifts have been denoted δ_L for each of the three initial channels, the CSB phase shifts are denoted $\bar{\delta}_L$ for the $^1P_1$ and $^3D_2$ channels, and the coupled channel phase shifts are $\bar{\delta}_\alpha$ and $\bar{\delta}_\beta$. Because the $^3S_1$ and $^3D_1$ channels are coupled, $\overline{B}$ and $\overline{C}$ are split into α and β parts

TABLE III. Strong reduced matrix elements.

Diagram	A_0	A_2	B	C
Impulse (w/wfn corr)	0	0	−6.59	32.85
Impulse recoil	−5.62	−0.21	1.17	−8.56
RS (w/recoil)	81.12	0	0.54	1.66
Δ (no cutoff)	0	0	−33.94	37.96
Δ ($\Lambda = 417$ MeV)	0	0	−10.48	21.60

TABLE IV. CSB reduced matrix elements.

Diagram	$\overline{A}_0$	$\overline{A}_2$	$\overline{B}_\alpha$	$\overline{B}_\beta$	$\overline{C}_\alpha$	$\overline{C}_\beta$	$\overline{D}$
Impulse ($\times\frac{1}{\beta_1}$)	0	0	12.23	29.72	−7.80	−15.05	−28.30
RS ($\times\frac{100\text{MeV}}{\delta m_N^{\text{str}}}$)	−28.83	0	−1.37	1.79	1.48	1.89	−4.92
Δ ($\times\frac{1}{\beta_1}$)	0	0	12.60	−7.71	−8.47	−2.86	22.37

which have different phase shifts in the presence of initial state interactions.

Finally, for comparison purposes we include a translation between our reduced matrix elements and those of Ref. [20],

$$\begin{aligned} C_0 &= -\frac{1}{\sqrt{4\pi}} A_0 e^{i\delta_0} \\ C_1 &= -i\frac{1}{\sqrt{6\pi}} B e^{i\delta_1} \\ C_2 &= i\sqrt{\frac{3}{4\pi}} C e^{i\delta_2}, \end{aligned} \tag{B7}$$

where the C's are $pp \to d\pi^+$ amplitudes and isospin symmetry has been used to determine the translations.

APPENDIX C: DIAGRAM TECHNIQUE

To establish the diagram technique, consider Fig. 14 in light of Eq. (5). We write down the amplitude using momentum space Feynman rules, Fourier transform, and then convolve with the initial and final state wave functions. The left line is taken to be "nucleon 1" and we make the approximation that the exchanged pion carries half of the produced pion's energy, $q' = (\omega_q/2, \vec{q}')$. Momentum conservation gives $\vec{q}' = \vec{k} - \vec{p} + \vec{q}/2$. According to Eq. (A1) the WT vertex contributes $1/(4f_\pi^2)\tau_{1,b}\epsilon_{a3b}(\omega_q/2 + \omega_q)$ and the πNN vertex contributes $g_A/(2f_\pi)\tau_{2,a}\vec{\sigma}_2 \cdot (-\vec{q}')$. The momentum space propagator is $-i/(\vec{q}'^2 + \mu^2)$, where $\mu^2 = m_\pi^2 - \omega_q^2/4$ is the effective mass of the rescattered pion. Next, as discussed in Sec. III A, we

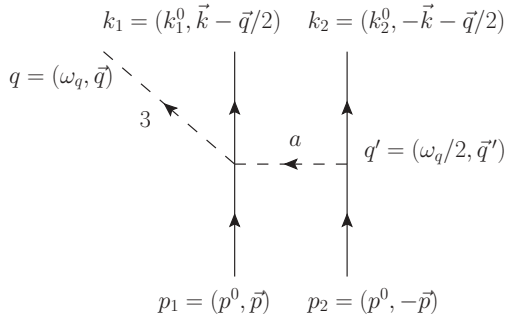

FIG. 14. Strong rescattering diagram. Solid lines represent nucleons, dashed lines represent pions, and the pions' isospin z components are labeled 3 and a.

Fourier transform with respect to $\vec{l} = \vec{k} - \vec{p}$,

$$\begin{aligned} \int \frac{d^3l}{(2\pi)^3} e^{i\vec{l}\cdot\vec{r}} \frac{\vec{\sigma}_2 \cdot \vec{q}'}{\vec{q}'^2 + \mu^2} &= e^{-i\vec{q}\cdot\vec{r}/2} \int \frac{d^3q'}{(2\pi)^3} e^{i\vec{q}'\cdot\vec{r}} \frac{\vec{\sigma}_2 \cdot \vec{q}'}{\vec{q}'^2 + \mu^2} \\ &= e^{-i\vec{q}\cdot\vec{r}/2} \vec{\sigma}_2 \cdot (-i\vec{\nabla}) \frac{e^{-\mu r}}{4\pi r} \\ &= \frac{i\mu}{4\pi} e^{-i\vec{q}\cdot\vec{r}/2} h(r) \vec{\sigma}_2 \cdot \hat{r}, \end{aligned} \tag{C1}$$

where $h(r) \equiv (1 + 1/\mu r)e^{-\mu r}/r$.

The deuteron has isospin 0 and the np wave fuction includes a $T = 1$, $T_z = 0$ isospinor $|1, 0\rangle$, and thus

$$\langle 0, 0 | i\epsilon_{a3b}\tau_{1,b}\tau_{2,a} | 1, 0\rangle = -2. \tag{C2}$$

At this point, we have (defining $\hat{\mathcal{M}}' = \hat{\mathcal{M}}/\sqrt{2E_1 2E_2 2E_d}$)

$$\langle 0, 0 | \hat{\mathcal{M}}'_L | 1, 0\rangle = -i\frac{g_A}{2f_\pi} \frac{3\omega_q/2}{8\pi f_\pi^2} \mu h(r) e^{-i\vec{q}\cdot\vec{r}/2} \vec{\sigma}_2 \cdot \hat{r}. \tag{C3}$$

To calculate the diagram with the WT vertex on nucleon 2, we consider how each part of the left side of Eq. (C3) transforms under $1 \leftrightarrow 2$. Because the strong part of the Lagrangian is invariant under isospin, $\hat{\mathcal{M}}$ is invariant. The initial isospin ket $|1, 0\rangle$ is invariant as well, but $|0, 0\rangle \to -|0, 0\rangle$. Also note that $\vec{r} \to -\vec{r}$. Thus,

$$\langle 0, 0 | \hat{\mathcal{M}}'_R | 1, 0\rangle = -i\frac{g_A}{2f_\pi} \frac{3\omega_q/2}{8\pi f_\pi^2} \mu h(r) e^{i\vec{q}\cdot\vec{r}/2} \vec{\sigma}_1 \cdot \hat{r}. \tag{C4}$$

Defining $\vec{S} \equiv (\vec{\sigma}_1 + \vec{\sigma}_2)/2$, $\vec{\Sigma} \equiv (\vec{\sigma}_1 - \vec{\sigma}_2)/2$ and

$$\begin{aligned} \mathcal{E} &\equiv \exp(i\vec{q}\cdot\vec{r}/2) + \exp(-i\vec{q}\cdot\vec{r}/2) \\ \mathcal{O} &\equiv \exp(i\vec{q}\cdot\vec{r}/2) - \exp(-i\vec{q}\cdot\vec{r}/2), \end{aligned} \tag{C5}$$

we have the complete rescattering operator,

$$\langle 0, 0 | \hat{\mathcal{M}}'_{\text{RS}} | 1, 0\rangle = -i\gamma_{\text{RS}} h(r) (\mathcal{E}\vec{S} \cdot \hat{r} + \mathcal{O}\vec{\Sigma} \cdot \hat{r}), \tag{C6}$$

where

$$\gamma_{\text{RS}} \equiv \frac{g_A}{2f_\pi} \frac{3\omega_q/2}{8\pi f_\pi^2} \mu. \tag{C7}$$

To proceed, we preform a partial wave expansion on $\mathcal{E}$ and $\mathcal{O}$ and just keep the leading term. Note that we use the coordinate system defined by $\hat{q} = \hat{z}$. Then we calculate the spin-angle matrix elements of the rank zero $\mathcal{E}\vec{S} \cdot \hat{r}$ and the rank one $\mathcal{O}\vec{\Sigma} \cdot \hat{r}$ operators. The final expression for $\langle f | \hat{\mathcal{M}} | i\rangle$ simplifies to a radial integral which is computed numerically. Note that the first term in Eq. (C6) corresponds to s-wave pions because $\mathcal{E}$ carries $L = 0$ and $\hat{r}$ carries $L = 1$, and thus the operator will change the parity. Likewise, the second

TABLE V. Strong phase shifts.

δ_1	−0.47
δ_0	−0.044
δ_2	0.16

term corresponds to p-wave pions. In terms of the reduced matrix elements of Eqs. (B1) and (B2), we have

$$\begin{aligned} A_0^{\rm RS} &= \sqrt{2E_1 2E_2 2E_d}\,8\pi\,\gamma_{\rm RS}\sqrt{2}K_1 \\ A_2^{\rm RS} &= 0 \\ B^{\rm RS} &= \sqrt{2E_1 2E_2 2E_d}\,8\pi\,\gamma_{\rm RS}\sqrt{3}K_0 \\ C^{\rm RS} &= \sqrt{2E_1 2E_2 2E_d}\,8\pi\,\gamma_{\rm RS}\sqrt{6}K_2, \end{aligned} \tag{C8}$$

where the integrals are defined

$$\begin{aligned} K_1 &\equiv \int dr\, r^2 \left[\frac{u_d(r)}{r} + \frac{w_d(r)}{\sqrt{2}r}\right] j_0\left(\frac{qr}{2}\right) h(r) \frac{u_{1,1}(r)}{pr} \\ K_0 &\equiv \int dr\, r^2 \left[\frac{u_d(r)}{r} - 2\frac{w_d(r)}{\sqrt{2}r}\right] j_1\left(\frac{qr}{2}\right) h(r) \frac{u_{0,0}(r)}{pr} \\ K_2 &\equiv \int dr\, r^2 \left[\frac{u_d(r)}{r} - 2\frac{w_d(r)}{\sqrt{2}r}\right] j_1\left(\frac{qr}{2}\right) h(r) \frac{u_{2,2}(r)}{pr}. \end{aligned} \tag{C9}$$

APPENDIX D: OBSERVABLES

One experimental observable is the analyzing power, A_y, defined in Eq. (21). In the strong sector, we find (neglecting A_2, which is numerically small)

$$A_y = \frac{\sqrt{3}\cos(\phi)\sin(\theta)A_0[\sqrt{2}B\sin(\delta_0-\delta_1)+C\sin(\delta_2-\delta_1)]}{3A_0^2+B^2+C^2+[C^2-2\sqrt{2}BC\cos(\delta_2-\delta_0)]P_2(\cos\theta)}, \tag{D1}$$

where the angular dependence is that of the nucleon relative momentum, $\vec{p}$, with respect to the pion momentum, $\hat{q} = \hat{z}$. To compare with experimental results, which use $\hat{p} = \hat{z}$ and $\phi_\pi = 0$, we need to set $\phi_N = \pi$ and $\theta_N = \theta_\pi$.

To calculate the differential cross section as well as the asymmetry, we need to square the sum of all the matrix elements, sum over m_f and average over m_1 and m_2. First we define

$$\begin{aligned} &\frac{1}{4}\sum |\langle f|\hat{\mathcal{M}}^{\rm tot}|i\rangle|^2 \\ &\quad = M_0 + M_1 P_1(\cos\theta) + M_2 P_2(\cos\theta) + M_3 P_3(\cos\theta), \end{aligned} \tag{D2}$$

TABLE VI. CSB phase shifts.

$\overline{\delta}_1$	−0.44
$\overline{\delta}_\alpha$	0.19
$\overline{\delta}_\beta$	−0.43
$\overline{\delta}_2$	0.44

so that

$$\sigma = \frac{|\vec{q}|}{64\pi^2 s|\vec{p}|} 4\pi M_0 \tag{D3}$$

$$A_{\rm fb} = \frac{M_1 - \frac{1}{4}M_3}{2M_0}. \tag{D4}$$

The results for the required quantities are

$$\begin{aligned} M_0 = \frac{1}{48\pi}\Bigg[&3\left(A_0^2 + \overline{A}_0^2\right) + \frac{3}{5}\left(A_2^2 + \overline{A}_2^2\right) \\ &+ \left(B^2 + \overline{B}_\alpha^2 + \overline{B}_\beta^2 + C^2 + \overline{C}_\alpha^2 + \overline{C}_\beta^2 + \overline{D}^2\right) \\ &+ 2(\overline{B}_\alpha\overline{B}_\beta + \overline{C}_\alpha\overline{C}_\beta)\cos(\overline{\delta}_\alpha - \overline{\delta}_\beta)\Bigg] \end{aligned} \tag{D5}$$

$$\begin{aligned} M_1 = \frac{\sqrt{3}}{24\pi}\Bigg\{&B\left(\overline{A}_0 - 2\sqrt{\frac{1}{10}}\overline{A}_2\right)\cos(\overline{\delta}_1 - \delta_0) \\ &- \sqrt{2}C\left(\overline{A}_0 - \frac{1}{5\sqrt{10}}\overline{A}_2\right)\cos(\overline{\delta}_1 - \delta_2) \\ &+ \left(A_0 + \frac{1}{\sqrt{10}}A_2\right)\left[\left(\overline{B}_\alpha + \frac{1}{\sqrt{2}}\overline{C}_\alpha\right)\right. \\ &\left.\times\cos(\overline{\delta}_\alpha - \delta_1) + (\alpha \to \beta)\right] \\ &- \sqrt{\frac{3}{2}}\left(A_0 - \frac{1}{5\sqrt{10}}A_2\right)\overline{D}\cos(\overline{\delta}_2 - \delta_1)\Bigg\} \end{aligned} \tag{D6}$$

$$\begin{aligned} M_2 = \frac{1}{8\sqrt{10}\pi}\Bigg\{&(A_0A_2 - 2\overline{A}_0\overline{A}_2) - \frac{1}{2\sqrt{10}}\left(A_2^2 - 2\overline{A}_2^2\right) \\ &+ \frac{5}{3\sqrt{10}}\Bigg[C^2 - \frac{1}{2}\overline{C}_\alpha^2 - \frac{1}{2}\overline{C}_\beta^2 + \frac{1}{2}\overline{D}^2 \\ &- \overline{C}_\alpha\overline{C}_\beta\cos(\overline{\delta}_\alpha - \overline{\delta}_\beta)\Bigg] \\ &- \frac{\sqrt{5}}{3}[2BC\cos(\delta_2 - \delta_0) - \overline{B}_\alpha\overline{C}_\alpha \\ &- \overline{B}_\beta\overline{C}_\beta - (\overline{B}_\alpha\overline{C}_\beta + \overline{B}_\beta\overline{C}_\alpha)\cos(\overline{\delta}_\alpha - \overline{\delta}_\beta)] \\ &- \sqrt{\frac{5}{3}}\left(\overline{B}_\alpha + \frac{1}{\sqrt{2}}\overline{C}_\alpha\right)\overline{D}\cos(\overline{\delta}_2 - \overline{\delta}_\alpha) - (\alpha \to \beta)\Bigg\} \end{aligned} \tag{D7}$$

$$M_3 = \frac{3}{40\pi}\sqrt{\frac{3}{5}}\left[C\overline{A}_2\cos(\overline{\delta}_1 - \delta_2) - \frac{1}{\sqrt{3}}A_2\overline{D}\cos(\overline{\delta}_2 - \delta_1)\right]. \tag{D8}$$

Disregarding the small M_3 term, the asymmetry is proportional to Eq. (D6). The physical content of Eq. (D6)'s first two lines is the interference of strong p-wave pions with CSB s-wave pions while the content of the last three lines is strong s-wave and CSB p-wave.

Table III shows the strong reduced matrix elements and Table IV the CSB reduced matrix elements. The CSB rescattering numbers were calculated including the new contributions discovered by Ref. [14]. The np phase shifts (in radians) that appear in the cross section according to Eqs. (D5)–(D8) are given in Tables V and VI.

[1] E. E. Jenkins and A. V. Manohar, Phys. Lett. **B255**, 558 (1991).
[2] S. Weinberg, Nucl. Phys. **B363**, 3 (1991).
[3] V. Bernard, N. Kaiser, and U. G. Meissner, Z. Phys. C **60**, 111 (1993).
[4] T. R. Hemmert, B. R. Holstein, and J. Kambor, J. Phys. G **24**, 1831 (1998).
[5] C. Y. Cheung, E. M. Henley, and G. A. Miller, Nucl. Phys. **A348**, 365 (1980).
[6] E. Epelbaum and U.-G. Meissner, Phys. Lett. **B461**, 287 (1999).
[7] G. A. Miller, A. K. Opper, and E. J. Stephenson, Annu. Rev. Nucl. Part. Sci. **56**, 253 (2006).
[8] I. Slaus, B. M. K. Nefkens, and G. A. Miller, Nucl. Instrum. Methods B **56-57**, 489 (1991).
[9] S. Weinberg, Trans. New York Acad. Sci. **38**, 185 (1977).
[10] A. K. Opper *et al.*, Phys. Rev. Lett. **91**, 212302 (2003).
[11] V. Lensky *et al.*, Eur. Phys. J. A **27**, 37 (2006).
[12] J. A. Niskanen, Few-Body Syst. **26**, 241 (1999).
[13] U. van Kolck, J. A. Niskanen, and G. A. Miller, Phys. Lett. **B493**, 65 (2000).
[14] A. Filin *et al.*, Phys. Lett. **B681**, 423 (2009).
[15] T.-S. Park, K. Kubodera, D.-P. Min, and M. Rho, Nucl. Phys. **A684**, 101 (2001).
[16] R. B. Wiringa, V. G. J. Stoks, and R. Schiavilla, Phys. Rev. C **51**, 38 (1995).
[17] C. Hanhart, Phys. Rep. **397**, 155 (2004).
[18] D. A. Hutcheon *et al.*, Phys. Rev. Lett. **64**, 176 (1990).
[19] A. Gardestig, D. R. Phillips, and C. Elster, Phys. Rev. C **73**, 024002 (2006).
[20] V. Baru, E. Epelbaum, J. Haidenbauer, C. Hanhart, A. E. Kudryavtsev, V. Lensky, and U. G. Meissner, Phys. Rev. C **80**, 044003 (2009).
[21] C. Hanhart, U. van Kolck, and G. A. Miller, Phys. Rev. Lett. **85**, 2905 (2000).
[22] P. Heimberg *et al.*, Phys. Rev. Lett. **77**, 1012 (1996).
[23] U. van Kolck, Few-Body Syst. Suppl. **9**, 444 (1995).
[24] J. Gasser and H. Leutwyler, Phys. Rep. **87**, 77 (1982).
[25] U. van Kolck, J. L. Friar, and J. T. Goldman, Phys. Lett. **B371**, 169 (1996).
[26] S. A. Coon and M. D. Scadron, Phys. Rev. C **51**, 2923 (1995).
[27] T. S. Park *et al.*, Phys. Rev. C **67**, 055206 (2003).
[28] T. D. Cohen, J. L. Friar, G. A. Miller, and U. van Kolck, Phys. Rev. C **53**, 2661 (1996).